Rat liver peroxisomes after fibrate treatment - A survey using quantitative mass spectrometry

Islinger, M.; Luers, G.H.; Li, K.W.; Loos, M.; Volkl, A.

published in
Journal of Biological Chemistry
2007

DOI (link to publisher)
10.1074/jbc.M610910200

document version
Publisher's PDF, also known as Version of record

THE JOURNAL OF BIOLOGICAL CHEMISTRY VOL. 282, NO. 32, pp. 23055–23069, August 10, 2007

Rat Liver Peroxisomes after Fibrate Treatment

A SURVEY USING QUANTITATIVE MASS SPECTROMETRY[*] [S]

Received for publication, November 27, 2006, and in revised form, May 16, 2007 Published, JBC Papers in Press, May 22, 2007, DOI 10.1074/jbc.M610910200

Markus Islinger[‡1,2], **Georg H. Lüers**[§1], **Ka Wan Li**[¶], **Maarten Loos**[¶], **and Alfred Völkl**[‡]

From the [‡]*Department of Anatomy and Cell Biology, Ruprecht-Karl University, 69120 Heidelberg, Germany, the* [§]*Department of Anatomy and Cell Biology, Phillips-University, 35033 Marburg, Germany, and the* [¶]*Research Institute of Neurosciences, Vrije Universiteit, 1081 HV Amsterdam, Netherlands*

Fibrates are known to induce peroxisome proliferation and the expression of peroxisomal β-oxidation enzymes. To analyze fibrate-induced changes of complex metabolic networks, we have compared the proteome of rat liver peroxisomes from control and bezafibrate-treated rats. Highly purified peroxisomes were subfractionated, and the proteins of the matrix, peripheral, and integral membrane subfractions thus obtained were analyzed by matrix-assisted laser desorption ionization time-of-flight/time-of-flight mass spectrometry after labeling of tryptic peptides with the iTRAQ reagent. By means of this quantitative technique, we were able to identify 134 individual proteins, covering most of the known peroxisomal proteome. Ten predicted new open reading frames were verified by cDNA cloning, and seven of them could be localized to peroxisomes by immunocytochemistry. Moreover, quantitative mass spectrometry substantiated the induction of most of the known peroxisome proliferator-activated receptor α-regulated peroxisomal proteins upon treatment with bezafibrate, documenting the suitability of the iTRAQ procedure in larger scale experiments. However, not all proteins reacted to a similar extent but exerted a fibrate-specific induction scheme showing the variability of peroxisome proliferator-activated receptor α-transmitted responses to specific ligands. In view of our data, rat hepatic peroxisomes are apparently not specialized to sequester very long chain fatty acids (C22–C26) but rather metabolize preferentially long chain fatty acids (C16–18).

Peroxisomes, often described as multipurpose organelles, are involved in numerous biochemical pathways of lipid and peroxide metabolism. The existence of more than 15 peroxisomal inherited diseases like the Zellweger syndrome or X-linked adrenoleukodystrophy, which are often lethal, emphasizes the vital importance of these organelles (1–3). Cells are able to remodel the protein composition of their peroxisomes and to adjust the number of these organelles in response to physiological or environmental stimuli to cope with the metabolic needs. Consequently, peroxisomes are regarded as highly modular organelles, with different protein composition depending on the metabolic function or cell type. Fibrates, used as hypolipidemic drugs, induce both the proliferation of peroxisomes as well as the β-oxidation of fatty acids (4). These alterations of the metabolic functions of peroxisomes are accompanied by changes of proteins involved in the biogenesis of the organelles as well as in enzymes for the breakdown of fatty acids (5, 6). Several investigators in the past have used fibrate-induced peroxisome proliferation as a model to analyze selected aspects of peroxisome biogenesis or lipid metabolism, using techniques like Western blotting, enzyme assays, immunocytochemistry, Northern blotting, or *in situ* hybridization (6–11). However, complex rearrangements of the entire peroxisomal proteome could not be analyzed with these techniques.

In this respect, mass spectrometry represents a straightforward alternative, particularly because of the development of more sensitive analyzers and the introduction of isotope labeling reagents (12). Thus, it is now possible to characterize the different physiological states of an organelle structure by top-down quantitative mass spectrometry because of its ability to identify hydrophobic polypeptides, like integral membrane proteins (13–16), to investigate quantitative changes of individual proteins, even of low abundance, by the use of stable isotope-labeled tags (17), and to record modulations of selected pathways in response to exogenous stimuli. Last but not least, it enables the identification of previously undetected proteins and their integration into a cellular network as a basis for further functional studies.

Because of their small proteome, peroxisomes represent a model of comparably low complexity suitable to use quantitative MS[3] in a functional approach. By using this technique, we have analyzed the peroxisomal proteome in response to fibrate treatment with the aim to elucidate complex proteome rearrangements, to identify undetected proteins, and to define their subcellular location and organelle-specific functions. In our analysis we isolated peroxisomes from bezafibrate-treated and control rats by means of density gradient centrifugation using a

* This work was supported by the German Federal Ministry for Education and Research FKZ 031U108F (subproject B5). The costs of publication of this article were defrayed in part by the payment of page charges. This article must therefore be hereby marked "*advertisement*" in accordance with 18 U.S.C. Section 1734 solely to indicate this fact.

[S] The on-line version of this article (available at http://www.jbc.org) contains supplemental Figs. S1 and S2.

[1] Both authors contributed equally to this work.

[2] To whom correspondence should be addressed: Dept. of Anatomy and Cell Biology, Medical Cell Biology, University of Heidelberg, Im Neuenheimer Feld 307, 69120 Heidelberg, Germany. E-mail: Markus.Islinger@urz.uni-heidelberg.de.

[3] The abbreviations used are: MS, mass spectrometry; ACOX1, acyl-CoA oxidase 1; D-PBE, peroxisomal D-bifunctional enzyme; L-PBE, peroxisomal L-bifunctional enzyme; Tysnd1, trypsin domain containing 1; ACBD, acyl-CoA binding domain; MS/MS, tandem mass spectrometry; CHO, Chinese hamster ovary; PBS, phosphate-buffered saline; MOPS, 4-morpholinepropanesulfonic acid; GFP, green fluorescent protein; PPAR, peroxisome proliferator-activated receptor; ALDP, adrenoleukodystrophy protein.

standardized procedure (18). To further increase the precision of the analysis, isolated peroxisomes were carefully subfractionated into matrix and peripheral as well as integral membrane protein fractions to enrich low abundant proteins. The proteins were directly digested with trypsin and labeled with iTRAQ reagent for quantitative liquid chromatography-MS/MS analysis. Thus, we were able to identify 134 proteins, including 15 new predicted open reading frames. Ten of them could be verified by cDNA cloning, and seven were shown to localize at least partially to peroxisomes. The quantitative assessment of protein abundance in response to the fibrate treatment revealed no new fibrate-induced protein species. Convincing evidence, however, is provided by the quite distinct induction rates of long chain fatty acid synthetase and PMP70 in contrast to very long chain fatty acid synthetase and ALDP and the finding that long chain fatty acids (C16–C18) rather than very long chain fatty acids (C22–C26) are the primary substrates of rat liver peroxisomes after fibrate treatment.

EXPERIMENTAL PROCEDURES

Maintenance and Bezafibrate Treatment of Rats—Female Sprague-Dawley rats (200–300 g) were kept in accordance with the guidelines of the humane care and use of laboratory animals at the Zentrale Versuchstieranlage, University of Heidelberg, Germany. Each of 50 animals was fed for 10 days with 20 g of Altromin 1324 (Altromin International, Lage, Germany) containing 1 mg/g bezafibrate (Roche Diagnostics), equaling a dose of ~75 mg/kg body weight. The control group of 70 animals was fed with the same amount of untreated Altromin 1324. After the 10-day treatment, the animals were starved overnight and anesthetized with chloral hydrate. Subsequently, livers were excised, weighed, and minced in ice-cold homogenization buffer (250 mM sucrose, 5 mM MOPS, 1 mM EDTA, 0.1% ethanol, 2 mM phenylmethylsulfonyl fluoride, 1 mM dithiothreitol, 1 mM ϵ-aminocaproic acid, pH 7.2).

Isolation and Subfractionation of Peroxisomes—Homogenization of the tissue and subcellular fractionation was performed according to Völkl and Fahimi (18) with a few modifications described by Weber and co-workers (19). Finally, purified peroxisomes were washed once with gradient buffer (5 mM MOPS, 1 mM EDTA, 0.1% ethanol, 2 mM phenylmethylsulfonyl fluoride, 1 mM dithiothreitol, 1 mM ϵ-aminocaproic acid, pH 7.2) and stored at −80 °C. For subfractionation into matrix, peripheral, and integral membrane compartments, peroxisomes were thawed and centrifuged at 30,000 × *g*, resulting in supernatant S1 and pellet P1. P1 was resuspended in TVBE buffer (1 mM Na_2CO_3, 1 mM EDTA, 0.1% ethanol, 0.01% Triton X-100, pH 7.6), supplemented to 0.1% Triton and sonicated with two 15-s pulses at 100 watts for quantitative membrane disruption. Thereafter, a second centrifugation step at 100,000 × *g* for 30 min, resulted in a first membrane pellet (P2) and supernatant S2. To remove peripherally attached proteins, P2 was suspended in 250 mM KCl and centrifuged again at 100,000 × *g* (S3 and P3). Subsequently, P3 was suspended in 100 mM Na_2CO_3 and kept on ice for 30 min. After a final centrifugation at 100,000 × *g*, the supernatant (S4), containing mainly the core protein urate oxidase (>90%), was discarded, and the integral membrane pellet (P4) was washed and stored in gradient buffer. For the matrix fraction, S1 and S2 were combined, concentrated with VivaSpin columns (MW 5000, Sartorius, Goettingen, Germany), and dialyzed in gradient buffer. Supernatant S3 was concentrated and dialyzed in the same way to obtain a fraction of peripherally attached membrane proteins.

iTRAQ Labeling and Liquid Chromatography-MS/MS—To ensure that equal protein amounts were subjected to iTRAQ labeling, first protein concentrations of the subfractions were determined by the Bradford method. For a more precise comparison of protein amounts in the membrane fractions, aliquots of all three subfractions were run on an SDS gel and stained with Coomassie Blue. Thereafter, staining intensity of the protein pattern was compared by densitometric analysis of the gel (Quantity One Software, Bio-Rad). Peroxisomal proteins (100 μg per sample) were trypsin-digested (membrane pellets were first solubilized in 0.8% RapiGest, Waters) and tagged with iTRAQ reagents according to the protocol provided by the manufacturer (Applied Biosystems). The iTRAQ-labeled peptides were resolved in the first-dimensional liquid chromatography with a polysulfoethyl A column. Peptides were eluted with a linear gradient of 0–500 mM KCl in 20% acetonitrile, 10 mM KH_2PO_4, pH 2.9, over 25 min at a flow rate of 50 μl/min. Fractions were collected at 1-min intervals, dried, and redissolved in 30 μl of 0.1% trifluoroacetic acid. For the second-dimensional liquid chromatography, 10 μl were injected into a capillary C18 column (150 × 100 mm inner diameter. column) at 500 nl/min and separated with a linearly increasing concentration of acetonitrile from 5 to 50% in 30 min and to 100% in 5 min. The eluent was mixed with matrix (7 mg of α-cyanohydroxycinnaminic acid in 1 ml of 50% acetronitrile, 0.1% trifluoroacetic acid, 10 mM dicitrate ammonium) delivered at a flow rate of 1.5 ml/min and deposited off-line to the Applied Biosystems metal target every 15 s for a total of 192 spots, and analyzed on an ABI 4700 proteomics analyzer. Peptide CID was performed at 1 kV; the collision gas was nitrogen. MS/MS spectra were collected from 5000 laser shots. The peptides with signal to noise ratio above 50 at the MS mode were selected for MS/MS experiment; a maximum of 30 MS/MS was allowed per spot. The precursor mass window was 180 relative resolution (at full width half-maximum). MS/MS spectra were searched against the rat and mice data bases (Celera Discovery System, CDS) using GPS Explorer (ABI) and Mascot (MatrixScience) with trypsin specificity and fixed iTRAQ modifications at lysine residue and the N termini of the peptides. Mass tolerance was 100 ppm for precursor ions and 0.5 Da for fragment ions; one missed cleavage was allowed. For each MS/MS spectrum, a single peptide annotation with the highest Mascot score was retrieved. CDS protein sequence redundancy was removed by clustering the precursor protein sequences of the retrieved peptides using the cluster algorithm Cd hit (20) at a sequence similarity threshold of 90%. Subsequently, all peptides were matched against the obtained protein clusters; those peptides that matched more than one protein cluster represent common sequences between proteins and were not considered for protein identification and quantification. For quantification, peak areas for each iTRAQ signature peak were obtained and corrected according to the manufacturer's instruction to account for the differences in isotopic overlap. To compensate for the

TABLE 1
Plasmid constructs used for microscopic investigations

Protein name	Abbreviation used in text	Protein accession number	GenBank™ accession number of cDNA	Wild type	N-terminal tag	C-terminal tag
Acyl-CoA dehydrogenase family member 11		Q80XL6	XM_236582	−	Myc	−
δ3,δ2-Enoyl-CoA isomerase		NP_001009275	BC088178.1	−	Myc	−
Zinc-binding alcohol dehydrogenase domain containing 2	Zn-ADH	XP_214526	XM_001060611	−	Myc	−
Mosc domain containing protein 2	MOSC2	O88994	AF095741.1	−	Myc	Myc
Trypsin domain containing 1	Tysnd1	XP_345107.1	XM_001056113.1	−	Myc	−
PMP52	PMP52	NP_001013918	NM_001013896	+	Myc	Myc
Short chain dehydrogenase 7b	Dhrs7b	XP_213317.1	BC086453.1	−	Myc	Myc
	Dhrs7b.2		EF445633		Myc	Myc
Acyl-CoA-binding protein ACBD5	ACBD5.1	XP_237252.1	EF026991	+	Myc	Myc
	ACBD5.2		EF026992		Myc	Myc
Potential dienelactone hydrolase		NP_001008770.1	BC088459.1	−	Myc	Myc
Lactamase, β2		NP_663356	NM_001024247.1	−	Myc	−
Ezrin-radixin-moesin-binding phosphoprotein	EBP 50	Q9JJ19	AF154336.1	−	Myc	−

possible variation in the starting amount between the samples, the individual peak areas of each iTRAQ signature peak were $\log_2$-transformed to obtain a normal distribution and then normalized to the total peak area of this signature peak. Low signature peaks generally have larger variation, which may compromise the quantitative analysis of the proteins. Therefore, the iTRAQ signature peaks lower than 2000 were removed from quantitation. Within an MS experiment a Student's *t* test was used over bezafibrate *versus* control groups.

In the mass spectrometry, samples of peripheral and integral membrane proteins were run in parallel to obtain quantitative information on proteins retained at the membrane after carbonate stripping (data not shown). Because most of the proteins detected in the peripheral fraction were found in the matrix as well but specifically enriched proteins were not detected, the data for these subgroups were combined in Table 4. The ratio obtained for individual proteins identified in both groups was used to calculate a conjoint value for the induction in both subfractions to reduce data complexity. The mass spectrometry of the peroxisomal matrix was done independently, in a double experiment, and hence the quantitative measurements are shown as autonomous data. As a threshold for proteins presented, we used the identification of at least three peptides with the ion score of the highest peptide match >95% or two peptides with the highest peptide match >99%. For completion, some known peroxisomal proteins with identification rates below the threshold (indicated in Table 4) were included in the lists, because of the high probability of detection in a fraction of isolated peroxisomes. Nevertheless, only proteins detected with at least three peptides (peak area > 2000) were considered for quantification.

Immunoblotting of Selected Peroxisomal Proteins and Enzyme Assays—Western blotting was performed according to the semi-dry method using polyvinylidene difluoride membranes (21). Antibodies used for the immunodetection of selected proteins are of rabbit origin and were raised as published previously (uricase, PMP70, catalase, L-bifunctional enzyme, hydroxyacid oxidase, and acyl-CoA oxidase 1) or kind gifts from T. Hashimoto, Shinshu University School of Medicine, Nagano, Japan (long chain fatty acid CoA ligase 1, PMP22, and Pex11α), J. Adamski, GSF-Neuherberg, Germany (D-bifunctional enzyme), and G. Dodt, University of Tuebingen, Germany (Pex14). The polyclonal antibodies against GRP78/BiP and PECI were purchased from BD Biosciences.

The activity of acyl-CoA oxidase 1 (ACOX1) was determined according to Small *et al.* (22) and total β-oxidation activities as described by Lazarow and De Duve (4). Enzyme activities of catalase, esterase, cytochrome *c* oxidase, and acid phosphatase were performed as described previously (18).

Plasmids and Cloning of Expression Vectors for Newly Identified Peroxisomal Proteins—For the cloning of newly identified potential peroxisomal proteins, total rat liver RNA was isolated using RNeasy mini kit (Qiagen, Hilden, Germany) and reverse-transcribed into cDNA by SuperScript III reverse transcriptase (Invitrogen). Primers spanning the whole predicted open reading frame of the genes of interest were synthesized at MWG (München, Germany). PCR amplification of the target cDNAs was performed using *Pfx* polymerase (Invitrogen), and the amplicon was directly cloned into TOPO II vectors. After sequencing of the inserts (GATC, Konstanz, Germany), the open reading frames were isolated and ligated into pCMV-Tag vectors (Stratagene, Amsterdam, The Netherlands) for generation of fusions with the Myc epitope. For expression of Myc fusion proteins in mammalian cell lines, the coding regions were under control of the cytomegalovirus promoter. Except for protein sequences with predicted PTS1 signals at the C terminus where only N-terminal cDNA versions were constructed, both C- and N-terminally tagged versions were generated (see Table 1). For the analysis of wild-type protein variants, open reading frames of XP_237252.1 (ACBD5.2) and PMP52 were cloned into pCDNA3.1 vectors. In the case of XP_237252.1 (ACBD5) the 5′-end of the cDNA was determined using the GeneRacer RACE-PCR kit (Invitrogen). For cotransfection experiments, plasmid pDsRed (Clontech) or pGHL252 were used to visualize transgenic cells. The plasmid pGHL252 contains the sequence encoding a fusion protein (RFP-PTS1) of the red fluorescent protein (from pDsRed) with a peroxisomal targeting signal SKL under control of the murine ROSA26 promoter as well as an expression cassette for selection of bleomycin in prokaryotic and eukaryotic cells.

Cell Culture and Cell Lines—Chinese hamster ovary (CHO) cells and CHO-derived cells were maintained in Ham's F-12 medium supplemented with 10% fetal calf serum (PAA, Cölbe, Germany) in a fully humidified incubator at a temperature of

TABLE 2

Properties of the peroxisome fraction (PO) purified from livers of untreated rats

Values given are mean values ± S.D. Relative specific activity (RSA), units/mg PO protein × (units/mg liver protein)$^{-1}$. Purity/contamination of purified PO was calculated according the formula given by Leighton *et al.* (7): purity = $p \times$ RSA, where p is percentage of total liver protein contributed by PO (2.53).

Enzyme	No. of exp.	Units/g liver	Units/mg liver protein	Recovery in PO	Relative specific activity	Specific activity	Purity/contamination
		mg/g liver		*% total liver*		*Units/mg PO protein*	*%*
Protein	10	265.36 ± 81.84		0.28 ± 0.08			
Catalase	10	53.86 ± 11.34	202.96×10^{-3}	9.96 ± 1.92	37.67 ± 4.28	7.65	95.31
Lipid β-oxidation	4	0.951 ± 0.255	3.58×10^{-3}	11.18 ± 3.25	36.32 ± 5.09	0.130	91.89
β-Glucuronidase	4	10.12 ± 1.56	38.14×10^{-3}	0.014 ± 0.01	0.069 ± 0.056	0.003	0.139
Esterase	6	326.15 ± 65.46	1.229	0.014 ± 0.01	0.093 ± 0.07	0.114	1.99
Cytochrome *c* oxidase	8	33.10 ± 9.45	124.74×10^{-3}	0.018 ± 0.02	0.09 ± 0.05	0.011	1.82
Lactate dehydrogenase	2	448.15 ± 6.98	1.689	0.06	0.294	0.497	

37 °C and an atmosphere of 5% CO_2 in air. For visualization of peroxisomes in living cells, CHO cells were transfected with a mixture of plasmid pVgRXR (Invitrogen) and of plasmid pGHL97 (23) that contains an expression cassette for a GFP-PTS1 fusion protein under control of the murine phosphoglycerate kinase promoter. Cell clones were analyzed by fluorescence microscopy for expression of the GFP-PTS1 fusion protein, and positive clones were isolated for further analysis. One of the resulting cell clones with homogeneous expression of the GFP-PTS1 was named BGL69 and was used in this study.

Subcellular Localization of Epitope-tagged Proteins—For colocalization studies of epitope-tagged proteins with peroxisomes, expression vectors were transiently transfected into BGL69 cells cultured on glass coverslips using the Gene Porter system (Peqlab, Erlangen, Germany) according to the manufacturer's recommendations. After transfection, coverslips were washed with PBS and then fixed at room temperature in 4% freshly depolymerized paraformaldehyde in 0.15 M HEPES, pH 7.4, for 15 min. Cells were washed and permeabilized with 0.2% Triton X-100 and 0.2% Tween 20 in PBS. To reduce nonspecific binding of antibodies, cells were blocked for 30 min with Roti-Block (Roth, Karlsruhe, Germany) in PBS. Roti-Block was also used for dilution of specific primary and Cy3-labeled secondary antibodies. Cells were incubated with monoclonal primary antibodies against the Myc epitope (9E10, kindly provided by M. Schrader, University of Marburg, Germany) for 1 h. After washing the coverslips three times for 5 min, they were incubated with the Cy3-labeled goat anti-mouse antibodies (Dianova, Hamburg, Germany) for 1 h. Control stainings were performed according to the same protocol except that the primary antibodies were omitted. After a final washing, the coverslips were mounted with 50% glycerol in PBS containing 1.5% (w/v) *n*-propyl gallate as an antifade. For visualization of mitochondria, living CHO cells were incubated in Ham's F-12 medium supplemented with 0.5 μM MitoTracker Red (Invitrogen) for 30 min followed by an incubation in regular medium for 15 min. Cells were fixed and propagated for immunocytochemistry as described. For costaining of the Myc epitope in Mitotracker-labeled cells, the monoclonal anti-Myc antibodies were visualized using a Cy2-labeled goat anti-mouse antiserum (Dianova, Hamburg, Germany). Visualization of the endoplasmic reticulum with Concanavalin A was performed as described recently (23).

Light microscopic analysis was carried out on a Leica DMRE fluorescence microscope (Leica, Wetzlar, Germany) with standard filters for detection of fluorescein isothiocyanate and Cy3. Digital images were acquired using a DXM1200F digital camera system with the Nikon ACT-1 software.

RESULTS

Fibrates are known to induce hepatomegaly, to stimulate peroxisome proliferation, and to induce the enzymes involved in the β-oxidation of fatty acids (6). Accordingly, the bezafibrate treatment of animals was found to cause an increase in liver weight of 18.8% compared with untreated control animals (9.24 ± 1.06 *versus* 7.78 ± 0.64, $p < 0.001$). A more pronounced effect of the drug treatment was observed at the organellar level. Total peroxisomal protein increased from 26.5 to 102.4 μg/g liver, reflecting a 3.9-fold augmentation. Because this ratio was more or less consistent in all peroxisomal subfractions (matrix, 4.2, integral membrane fraction 3.3; peripheral membrane fraction, 3.7), peroxisomes were increased primarily in their number and to a lesser extent in size.

In Table 2, the properties of peroxisomes isolated in up to 10 experiments are summarized. According to the values concerning catalase and β-oxidation activities, the peroxisomal fractions obtained are highly enriched (purity of ~95%), with an average contamination by mitochondria and by endoplasmic reticulum of 2%, and hence are expected to meet the requirements for proteome analysis. To evaluate also the purity and contamination of peroxisomes isolated from bezafibrate-treated animals, we used the marker enzymes cytochrome *c* oxidase (mitochondria), esterase (endoplasmic reticulum), and acid phosphatase (lysosomes) to compare the former with "control peroxisomes." Because of the increase in peroxisome number in response to the treatment, most contaminating organelles decreased. In detail, the activities of cytochrome *c* oxidase were reduced by the factor of 3.4 and of esterase by 1.92, whereas that of acid phosphatase was augmented by the factor of 2.3 (Table 3), although no lysosomal proteins could be identified in the MS analysis.

To improve the precision of our MS analysis, isolated peroxisomes were subfractionated into so-called matrix, peripheral, and integral membrane fractions prior to MS/MS. Because peroxisomes exhibit a quite unique ratio of membrane to matrix (usually 1:10) and, moreover, are characterized by a portion of "poorly soluble" matrix proteins, which do not easily separate from the membrane (24), we had to adapt our subfractionation protocol to obtain a membrane preparation as pure as possible. For this purpose, we first disrupted the organelles by freezing and thawing in the presence of 0.075% Triton X-100, followed by sonication in 0.1% Triton X-100. Using this procedure, the

TABLE 3
Marker enzymes activities in isolated peroxisomes of bezafibrate-treated and control animals

Enzyme	Control	Bezafibrate
	Units/mg	*Units/mg*
Catalase	8.5	8.0
ACOX 1 (C18)	24.13	24.83
ACOX 1 (C24)	1.13	0.30
β-Oxidation (C18)	16.98 (milliunits/mg)	45.45 (milliunits/mg)
β-Oxidation (C24)	0.30 (milliunits/mg)	0.22 (milliunits/mg)
Unspecific esterase	0.140	0.073
Acidic phosphatase	0.096	0.223
Cytochrome *c* oxidase	0.017	0.005

matrix fraction was indeed enriched with the poorly soluble matrix proteins, *e.g.* the bifunctional enzymes (supplemental Fig. S1*a*), which was not possible with lower Triton X-100 concentrations. Yet, the Triton treatment also solubilized the integral membrane proteins to a minor extent (supplemental Fig. S1*b*), which was accepted to avoid contamination of the membrane fraction by matrix proteins. High salt KCl treatment is typically used for extraction of peripheral membrane proteins. However, because a complete clearance of poorly soluble matrix proteins from the membranes was not possible keeping detergent concentrations at an acceptable level, a distinct contamination of matrix proteins in the peripheral membrane fraction could not be avoided (supplemental Fig. S1*c*). In a last fractionation step the high abundant protein uricase was released from the membranes by washing with 100 mM carbonate. Concerning total protein amounts, we obtained the following distribution: matrix control, 12.6 mg; peripheral membranes control, 2 mg, integral membranes control, 1 mg; matrix bezafibrate, 46.3 mg; peripheral membranes bezafibrate, 5.6 mg; integral membranes bezafibrate, 3 mg.

Identification of Proteins Using MS/MS—After combining the analysis of all three peroxisomal subfractions, we were able to identify 134 different proteins or predicted peptide sequences (Table 4) matched from at least three peptides with an identification score of >95% or two peptides with >99%. Among these peptides were 57 *bona fide* peroxisomal proteins above that threshold as well as 18 microsomal, 16 mitochondrial, 15 cytosolic, 12 proteins of other sources, and 15 undefined peptide sequences (Table 4). With respect to the peroxisomal proteins, the mass spectrometric analysis reflected the biological function of peroxisomes in rat liver. The enzymes of lipid metabolism and the H_2O_2-degrading catalase were most prominent in the peroxisomal matrix subfraction judged from the ion scores and the number of peptides identified. High identification rates were also obtained for isocitrate dehydrogenase, strengthening the hypothesis of its role in generation of NADPH that is required for the breakdown of polyunsaturated fatty acids. Interestingly, we could verify the localization of only one enzyme of cholesterol biosynthesis supposed to be in peroxisomes, the hydroxymethylglutaryl-CoA synthase (Table 4). This may be an indication that the whole pathway of cholesterol synthesis is not localized in peroxisomes (25) and that the peroxisomal enzyme serves other tasks.

The mitochondrial glutathione *S*-transferase κ1, suggested to be a peroxisomal matrix protein (26), was one of the proteins detected with highest identification rates (peptide count 13, highest confidence interval per peptide 100%). Therefore, in addition to the enzymes scavenging reactive oxygen species like catalase and Cu,Zn superoxide dismutase (SOD1), peroxisomes contain high amounts of a third enzyme to protect the organelle from lipid peroxidation.

Within the peripheral membrane protein fraction, we did not find any peroxisomal proteins that were specifically enriched by bezafibrate. The membrane proteins were predominantly found in the carbonate-stripped protein fraction, including exclusively all newly identified proteins with predicted membrane-spanning helices according to TMHMM (Table 5). The major proteins found were the long chain fatty acid CoA ligase 1 (LACS1) and PMP70, both assigned to the function of fatty acid import (Table 4). According to the total ion score, very long chain acyl-CoA synthetase and ALDP are only present in low amounts in liver peroxisomes. In addition to proteins involved in lipid metabolism or transport of metabolites, we also detected nine peroxins. Pex2, -5, and -16, which were found but did not reach the identification threshold, were included in Table 4, because they are well characterized peroxisomal proteins, likely to be found in a peroxisomal protein sample.

We also detected proteins from other subcellular compartments in our proteome analysis. Their relative abundance varied depending on the original compartment. Mitochondrial proteins identified here generally belong to the respiratory chain or urea cycle and represent the most abundant proteins of this organelle. In contrast, microsomal and cytosolic proteins appeared to be part of distinct functional groups. Many of the microsomal proteins identified were chaperones and chaperone-related proteins. This selection of proteins suggests that they belong to a specialized microsomal subcompartment and were not just present because of a generalized microsomal contamination. Other proteins like the fatty aldehyde dehydrogenase, cytochrome b_5, and the NADH-cytochrome b_5 reductase (27–29) have already been described in peroxisomes and therefore may not be contaminants but proteins with a genuine partial peroxisomal localization.

The cytosolic proteins identified primarily belong to various pathways of energy metabolism and thus seem to be contaminants. However, the ezrin-radixin-moesin binding protein EBP50 possesses a PTS1 sequence at its C terminus implying a potential peroxisomal localization, which indeed could be confirmed by experiments described below.

Validation of Quantitative iTRAQ Data by Immunoblotting—The data acquired by iTRAQ analysis were validated by immunoblotting of selected peroxisomal proteins (Fig. 1). To perform a correlation analysis between both techniques, the intensities of bands were quantified using the Quantity One software (Bio-Rad). A correlation of all values acquired by both techniques resulted in a correlation coefficient of 0.62 (Excel, Microsoft). The overt inconsistencies between the iTRAQ and densitometry values may be caused by inaccuracies due to extremely low protein abundance in the sample. Thus, we excluded values from faint immunobands and/or iTRAQ data based on less than three peptides from the correlation analysis. After omitting these values the correlation coefficient rose to a value of 0.69. As a consequence, the semiquantitative evaluation of the

TABLE 4

List of protein identifications

A total of 134 proteins was identified with a threshold of three matching peptides, >95% probability for the peptide with the highest identification score or two peptide matches with a probability >99%. If a protein was found in the matrix and membrane fractions, the higher identification score was included into the list. iTRAQ values showing significant alterations according to a Student's *t* test are highlighted with the following color code: proteins up-regulated are shown in green and down-regulated proteins are highlighted in orange. Darker colors indicate changes of more than 100%. Proteins unaffected by the treatment are shown in yellow.

Localization	**Accesion No.**	*Name*	**Pep. Count.**	**Highest C.I p.p.**	**iTraq Mat.**	**iTraq Mmb**
peroxisomal						
Peroxisome biogenesis:	O70597	Peroxisomal membrane protein 11A, Pex11α	10	99.99	1.99	2.21
	Q9JJK4	Peroxisomal biogenesis factor 3, Pex3	6	100		1.43
	Q9Z2Z4	Peroxisomal membrane anchor protein Pex14	6	100		1.31
	XP_213746	Tetratricopeptide repeat protein 11 (Fis1p)	5	100	−1.17	
	O88177	Peroxisome assembly protein 12 (Pex12)	3	98.13	1.02	
	XP_233729.2	similar to Peroxisome assembly protein 10 (Pex10)	3	97.2		1.38
	BAA24931.1	Peroxisome assembly factor-2 (Pex6)	2	97.28		x
	NP_058930.1	Peroxisomal assembly factor-1 (Pex2)	1	100		x
	XP_242072.2	similar to peroxisome biogenesis factor 16 (Pex16)	1	99.53		x
	O09012	Peroxisomal targeting signal 1 receptor (Pex5)	1	95.81		x
β-oxidation:	P07896	Peroxisomal L-bifunctional enzyme (L-PBE)	42	100	4.24	2.68
	Q9Z1N0	Acyl-coenzyme A oxidase 1, peroxisomal (ACOX1)	37	100	1.11	−1.87
	P97852	Peroxisomal D-bifunctional enzyme (D-PBE)	30	100	1.21	1.27
	Q9QXD1	Acyl-coenzyme A oxidase 2, peroxisomal (ACOX2)	29	100	1.08	1.02
	P32020	Nonspecific lipid-transfer protein, SCPX/SCP2	19	100	−1.30	−1.42
	Q9EPL9	Acyl-coenzyme A oxidase 3, peroxisomal (ACOX2)	18	100	−1.42	−2.19
	P70473	Alpha-methylacyl-CoA racemase	15	100	−1.38	
	P07871	3-ketoacyl-CoA thiolase, peroxisomal	12	100	1.96	1.58
	Q8VHK0	Acyl-Coenzyme A thioesterase 8 ACOT8	4	97.23	1.29	
	Q8BWN8	Acyl-Coenzyme A thioesterase 4 ACOT4	3	99.99	2.17	1.70
α-oxidation	Q9QXE0	2-hydroxyphytanoyl-CoA lyase	17	100	−1.37	−1.14
	P57093	Phytanoyl-CoA dioxygenase, peroxisomal	17	100	1.07	−1.24
Oxid. polyunsat. fatty acids	Q9Z2M4	Peroxisomal 2,4-dienoyl-CoA reductase	16	100	1.52	1.10
	Q62651	δ3,5-δ2,4-dienoyl-CoA isomerase, mitochondrial	8	100	−1.42	1.27
	Q9WVK3	Peroxisomal trans-2-enoyl-CoA reductase	7	100	−1.15	1.14
	Q9WUR2	Peci protein (Enoyl CoA hydratase related)	6	100	−1.12	−1.24
Ketone body metabolism:	P97519	Hydroxymethylglutaryl-CoA lyase (HMG-CoA lyase)	8	100	−1.12	−1.19
Amino acid metabolism:	Q9D826	similar to Peroxisomal sarcosine oxidase	9	100	1.06	−1.27
	O35423	Serine-pyruvate aminotransferase	6	99.94	−1.31	−1.56
Bile acid synthesis:	Q63276	Kan-1 (Bile acid-CoA-amino acid N-acetyltransferase)	12	100	−1.51	−1.67
Purine metabolism:	P09118	Uricase EC 1.7.3.3	18	100	−1.64	−1.56
Fatty acid activat./transp.:	P16970	ATP-binding cassette sub-family D member 3, PMP70	31	100	−1.96	1.98
	P18163	Long-chain-fatty-acid-CoA ligase 1 (LACS1)	31	100	1.02	1.33
	Q704S8	Carnitine O-acetyltransferase	19	100	1.70	1.02
	P48410	ATP binding cassette sub-family D member 1, ALDP	7	100		1.45
	P02692	Fatty acid-binding protein, liver SCP p14	6	100	2.01	
	P11466	Peroxisomal carnitine O-octanoyltransferase (COT)	4	99.77	1.60	
	P97524	Very-long-chain acyl-CoA synthetase (VLACS)	4	96.34		1.32
Misc. membrane proteins:	Q07066	Peroxisomal membrane protein 2, (PMP22)	6	100	1.11	1.12
	P59382	Peroxisomal membrane protein 4 (PMP24)	5	100		1.19
	XP_216993.1	similar to PMP34 protein	1	99.60		x
Oxidation of redox equiv.:	O88844	Isocitrate dehydrogenase [NADP] cytoplasmic	24	100	1.01	
	P04642	L-lactate dehydrogenase A chain	15	100	−1.13	
	P05370	Glucose-6-phosphate 1-dehydrogenase (G6PD)	12	99.84		1.62
O_2 metabolism	P24270	Catalase	39	100	−1.56	1.79
	Q9WU19	Hydroxyacid oxidase 1	17	100	−1.24	1.49
	P24473	Glutathione S-transferase kappa 1	15	100	−1.18	−1.95
	O35078	D-amino-acid oxidase (DAMOX)	7	100	−1.68	
	P07632	Superoxide dismutase [Cu-Zn] (SOD1)	3	99.11	−1.37	
glycerolipid synthesis:	Q9ES71	Dihydroxyacetone phosphate acyltransferase	3	99.44		−1.01
Others:	XP_214655.2	peroxisomal Lon protease	6	100	−1.01	
	Q8VID1	Peroxisomal short-chain alcohol dehydrogenase 4	8	100	1.23	1.24
	P80299	Epoxide hydrolase 2	12	100	1.18	1.60
	P22791	Hydroxymethylglutaryl-CoA synthase	8	100	1.29	
	Q63716	Peroxiredoxin 1	4	99.94		−1.46
	P35559	Insulin-degrading enzyme	4	99.89	1.08	
	Q9DCN1	Peroxisomal NADH pyrophosphatase NUDT12	1	92.03		
microsomal:						
	P30839	Fatty aldehyde dehydrogenase EC 1.2.1.3	19	100	1.06	−1.15
	P09103	Protein disulfide-isomerase (Cellular thyroid hormone binding protein)	17	100	−1.28	
	P06761	78 kDa glucose-regulated protein (GRP 78, BiP)	11	100		1.66
	P20070	NADH-cytochrome b5 reductase EC 1.6.2.2	7	100	−1.07	
	P00173	Cytochrome b5	6	100	−1.75	1.90
	P50169	Retinol dehydrogenase 3	6	99.40	−1.40	
	O88813	Long chain fatty acid CoA ligase 5	6	98.13	−1.30	1.28
	P08113	94 kDa glucose-regulated protein (GRP94), Endoplasmin	5	99.6		1.46

TABLE 4—*continued*

Localization	Accesion No.	Name	Pep. Count.	Highest C.I p.p.	iTraq Mat.	iTraq Mmb
	P10867	L-gulonolactone oxidase	5	99.96	– 1.02	
	P18418	Calreticulin, ERp60	4	99.99	1.00	1.11
	P11598	Protein disulfide-isomerase A3, ERp60	4	100	– 1.14	
	XP_227765.2	similar to microsomal triglyceride transfer protein	4	99.99	– 1.06	
	P05178	Cytochrome P450 2C6 (CYPIIC6)	4	98.29	1.26	
	P07687	Epoxide hydrolase 1	3	100	1.07	
	P11711	Cytochrome P450 2A1 (CYPIIA1)	3	99.91	– 1.11	
	P08541	UDP-glucuronosyltransferase 2B2	2	100		x
	P11510	Cytochrome P450 2C12, female-specific (CYPIIC12)	2	99.97		x
	Q63010	Liver carboxylesterase 4	2	99.77	x	
mitochondrial						
	P07756	Carbamoyl-phosphate synthase, mitochondrial	15	100	– 1.15	1.25
	P10860	Glutamate dehydrogenase 1, mitochondrial	11	100	– 1.09	
	P32198	Carnitine O-palmitoyltransferase I, liver isoform	10	100	1.05	– 1.12
	O55171	Acyl-coenzyme A thioesterase 2 (ACOT2)	7	99.98	2.97	
	Q8BW75	Amine oxidase [flavin-containing] B	6	99.99	– 1.46	
	P15999	ATP synthase alpha chain, mitochondrial	6	99.60	– 1.74	– 1.06
	NP_036971.1	Cytochrome c, somatic	5	100		– 1.56
	P10719	ATP synthase beta chain, mitochondrial	5	99.99	– 2.03	
	P23965	d3,d2-trans-enoyl-CoA isomerase, mitochondrial	4	100		1.85
	P07824	Arginase-1	4	98.58		– 1.11
	P52759	Ribonuclease UK114	3	99.99	– 2.78	
	P09034	Argininosuccinate synthase	3	99.93		– 1.92
	P00481	Ornithine carbamoyltransferase	3	97.32	1.00	
	Q8BJ64	Choline dehydrogenase, mitochondrial	2	99.67	x	
	P09606	Glutamine synthetase	2	99.47		x
	Q64591	2,4-dienoyl-CoA reductase, mitochondrial	2	99.39	x	
cytosolic:						
	O35077	Glycerol-3-phosphate dehydrogenase [NAD+]	12	100	– 1.17	
	P04904	Glutathione S-transferase alpha 3, GST Yc-1	8	100	– 1.15	– 2.74
	Q99NB7	Acyl-Coenzyme A thioesterase 12 (ACOT 12)	8	100	– 1.03	
	P00884	Aldolase B, fructose-biphosphate	4	99.94		– 2.06
	O09171	Betaine--homocysteine S-methyltransferase	4	99.88		– 1.45
	P07936	Neuromodulin, Growth associated protein 43	4	99.86	1.06	
	P62630	Elongation factor 1-alpha 1	4	99.78		1.01
	P06757	Alcohol dehydrogenase A chain	3	100	1.06	– 1.25
	O88267	Cytosolic acyl coenzyme A thioester hydrolase, ind. (ACOT1)	3	99.99	2.69	
	Q9JJ19	Ezrin-radixin-moesin binding phosphoprotein , EBP50	3	99.99	– 2.38	x
	Q9JK72	Copper chaperone for superoxide dismutase (CCS)	3	99.19	x	
	P24368	Peptidyl-prolyl cis-trans isomerase A	3	99.89		– 1.05
	P13086	Succinyl-CoA ligase alpha chain	3	99.69		– 1.11
	P11232	Thioredoxin	2	99.99	– 1.37	
	P15626	Glutathione S-transferase Mu 2 (GSTM2-2)	2	99.50	1.05	
Undescribed:						
	Q80XL6	Acyl-CoA dehydrogenase family member 11	24	100	– 1.74	1.86
	NP_001009275	δ3, δ2-enoyl-CoA isomerase, (hypothetical protein LOC291076)	10	100	– 1.46	1.16
	O88994	Mosc domain containing protein 2 (MoCo sulfurase)	10	100	– 1.31	1.04
	XP_214526	Zinc binding alcohol dehydrogenase domain containing 2 (oxidoreductase activity, Zn-ADH))	6	100	– 1.35	
	NP_663356	Lactamase, beta 2	5	100	– 1.28	
	Q6I7R3	Isochorismatase domain-containing protein 1	5	100	– 1.16	
	XP_345107.1	Trypsin domain containing 1(Tysnd1, similar to hypothetical protein MGC34695)	4	99.99	– 1.19	1.13
	NP_001008770.1	Potential dienelactone hydrolase (hypothetical protein LOC310201)	4	99.98	1.30	
	NP_001013918	PMP52 (hypothetical protein LOC293098)	3	99.99	1.41	x
	AAH88229.1	LOC690745 protein MOSC N-terminal beta barrel domain	3	99.99	– 1.27	1.15
	Q6AY30	Probable saccharopine dehydrogenase	3	99.92	– 1.30	
	XP_213317.1	Short-chain dehydrogenase 7b (Dhrs7b, similar to DKFZP566O084 protein)	3	99.20		x
	XP_237252.1	Acyl-CoA binding protein ACBD5 (similar to RIKEN cDNA 1300014E15)	2	100		x

TABLE 4—*continued*

Localization	Accesion No.	Name	Pep. Count.	Highest C.I p.p.	iTraq Mat.	iTraq Mmb
	Q8VDX6	Transmembrane protein 5	2	99.13		x
	Q8CBY1	Sterile alpha motif domain-containing protein 4A	2	99.99	x	
Miscellaneous:						
	Q61092	Laminin gamma-2 chain precursor	9	99.99	−1.16	
	Q9EST6	Proliferation related acidic leucine rich protein PAL31	7	100		1.41
	P49290	Eosinophil peroxidase	6	99.44		−1.16
	AAH58508.1	protein for MGC:73009 (Splicing factor SC35)	5	100		−1.34
	P01946	Hemoglobin alpha-1/2 subunit, Alpha-1/2-globin	4	100	−1.18	−2.39
	P0C0T2	Ankyrin repeat and SAM domain containing protein 6	4	99.42		−1.39
	P62989	Ubiquitin	3	100		1.32
	Q63189	Eosinophil granule major basic protein prec. (MBP)	3	100		−1.46
	P02770	Serum albumin	3	99.82	1.09	
	Q06606	Granzyme-like protein II	3	99.75	1.22	
	P22734	Catechol O-methyltransferase	2	100		x
	Q69FB3	Junctophilin-4	2	99.64		x

TABLE 5

Molecular parameters of newly identified proteins

GenBank™ accession number	Name	PTS1 according to PTS1 predictor analysis software	No. of predicted membrane helices in TMHMM (GRAVY)	pI	M_r
Q80XL6	Acyl-CoA dehydrogenase family member 11	LQDQARQLKARM Yes, score 11.5	0 (−0.210)	8.40	87.37
NP_001009275.1	δ3,δ2-Enoyl-CoA isomerase	ALRNFLSRKAKI Yes, score 10.9	0 (−0.332)	8.57	33.69
XP_214526	Zinc-binding alcohol dehydrogenase domain containing 2	VVELPHPVSSKL Yes, score 2.7	0 (0.143)	7.63	40.48
O88994	Mosc domain-containing protein 2	LRVGDPVYRMVD No, score −2.7	1 (−0.210)	8.95	38.25
XP_345107.1	Trypsin domain-containing 1(Tysnd1)	QRPLPEAPRSKL Yes, score 13.8	0 (0.165)	6.50	58.99
NP_001013918	PMP52	TVVTPELPIDFS No, score −79.6	5 (0.178)	9.58	52.36
Q6I7R3	Isochorismatase domain-containing protein 1	ASAPESGLLSKV Yes, score 3.0	1 (−0.322)	6.96	32.00
XP_213317.1	Short chain dehydrogenase 7b	SRARKERKSKNS No, score −68.5	1 (0.072)	9.61	35.34
XP_23.7252.1	Acyl-CoA-binding protein ACBD5	HLYYQRRRRKLN No, score −55.3	1 (−0.651)	6.00	72.14
NP_001008770.1	Potential dienelactone hydrolase	RRNLIEWLNKYI No, score −27.9	0 (−0.268)	6.24	27.90
NP_663356	Lactamase β2	TTTPVKKWKAVL TwZ, score −3.9	0 (−0.302)	5.89	32.75
Q9JJ19	EBP50	DWSKKNELFSNL Yes, score 4.8	0 (−0.774)	5.70	38.83
Q8VDX6	Transmembrane protein 5	ILESSFFINNKV No, score −26.56	1 (−0.355)	8.89	51.39
Q6AY30	Probable saccharopine dehydrogenase	IQFSVISSSEVV No, score −87.54	1 (−0.038)	9.02	47.10
AAH88229.1	MOSC N-terminal β-barrel domain (LOC690745)	TIKVGDPVYLLS No, score −52.90	0 (−0308)	6.13	21.67
Q8CBY1	Sterile α motif domain-containing protein 4A	ALGDGVDRTSTI No, score −57.68	0 (−0.469)	8.61	69.04

bezafibrate treatment shown in Table 4 was based only on iTRAQ data of peroxisomal subfractions, in which proteins were detected by at least three peptides with a peak area >2000. Nevertheless, some inconsistencies were also evident for proteins, which were clearly detected by both techniques. For example, catalase is reduced in the matrix fraction according to the iTRAQ data, although it remained more or less stable in the immunoblots. Similarly, hydroxyacid oxidase is down-regulated in the iTRAQ analysis but induced according to the bands of the immunoblots. Both proteins were identified by more than 15 peptides, which means that more than 30 individual quantifications contributed to the iTRAQ value. To gain value of these data we performed a Student's *t* test in which only the data with significant variation was considered for subsequent interpretation. Otherwise, immunoblot quantification is based on the premise that exactly the same protein amounts have been loaded onto the gel. However, inaccuracies in the measurement of the protein concentration will lead to errors in the quantification of bands. In particular, this leads to problems in highly modulated protein samples like peroxisomes before and after fibrate treatment, because no housekeeping proteins can be used for validation. These problems can be avoided in the iTRAQ analysis, because protein amounts can be compensated virtually by the analysis software. Despite these drawbacks clear up- or down-regulations were detected in parallel as documented by the high induction rates of Pex11α, L-PBE, or PMP70

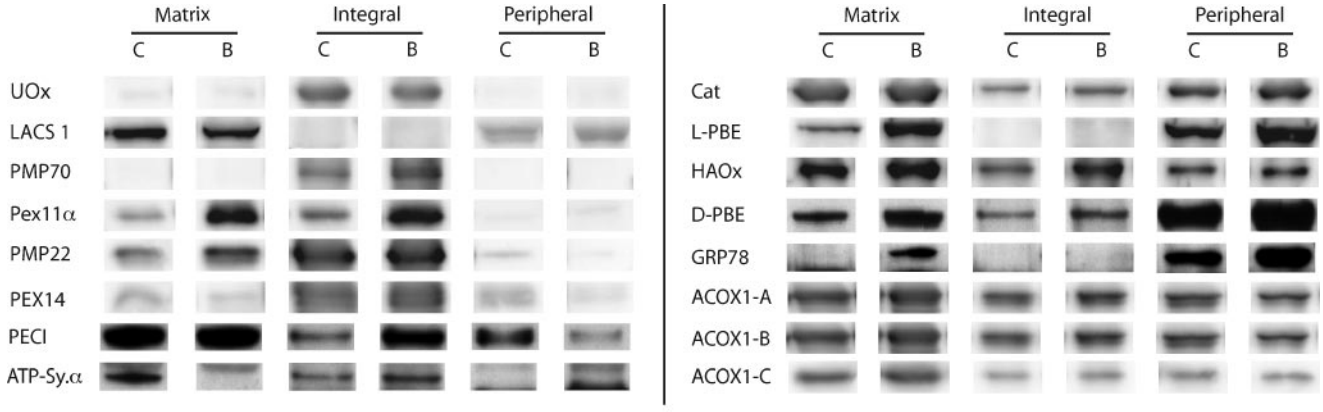

	Matrix		Integral		Peripheral	
	iTraq	*WB*	iTraq	*WB*	iTraq	*WB*
UOx	**0.61**	*1.06*	**0.63**	*0.81*	**0.79**	*1.36*
LACS 1	**1.02**	*1.02*	**1.32**	*1.09*	**1.39**	*1.09*
PMP70	**0.51**	*0.79*	**2.06**	*1.70*	**1.09**	*1.31*
Pex11α	**2.50**	*4.29*	**2.13**	*2.62*	**3.16**	*1.19*
PMP22	**1.11**	*1.91*	**1.10**	*0.84*	**1.72**	*0.44*
PEX14	**not id.**	*0.65*	**1.35**	*0.97*	**1.12**	*0.41*
PECI	**0.89**	*1.04*	**1.11**	*1.63*	**0.56**	*0.60*
ATP-Sy.α	**0.58**	*0.41*	**0.71**	*1.24*	**1.41**	*not id.*

	Matrix		Integral		Peripheral	
	iTraq	WB	iTraq	WB	iTraq	WB
Cat	**0.64**	*1.02*	**0.87**	*1.48*	**1.97**	*1.36*
L-PBE	**4.24**	*2.57*	**1.83**	*2.36*	**2.84**	*1.39*
HAOx	**0.81**	*1.08*	**0.87**	*1.60*	**1.82**	*1.11*
D-PBE	**1.21**	*1.54*	**1.46**	*1.35*	**1.25**	*1.24*
GRP78	**not id.**	*1.89*	**0.69**	*1.03*	**1.90**	*1.21*
ACOX1-A	**1.13**	*1.18*	**0.71**	*1.02*	**0.42**	*0.57*
ACOX1-B	**1.13**	*1.16*	**0.71**	*1.02*	**0.42**	*0.69*
ACOX1-C	**1.13**	*1.52*	**0.71**	*1.19*	**0.42**	*0.61*

FIGURE 1. **Immunoblots of selected proteins compared with iTRAQ ratios acquired by MS.** For the validation of the quantitative MS data, iTRAQ ratios (bezafibrate/control) are compared with band intensities of the immunoblots shown. Equal protein amounts of each peroxisomal subfraction were loaded on the gels, and after transfer to polyvinylidene difluoride membranes, individual proteins were detected by specific antibodies as described under "Experimental Procedures." For densitometry, Quantity One software (Bio-Rad) was used. The abbreviations used are as follows: *C,* control; *B,* bezafibrate; *Uox*, uricase; *LACS 1*, long chain fatty acid CoA ligase 1; *Cat*, catalase; *D-PBE*, L-bifunctional enzyme; *HAOx*, hydroxyacid oxidase; *D-PBE*, D-bifunctional enzyme; *ACOX1-A, -B, -C*, acyl-CoA oxidase 1, band 1, 2, and 3; *id*, identified.

found in both techniques. As a consequence, we focused the data interpretation on the clearly regulated proteins involved in the pathways of β-oxidation of fatty acids.

Bezafibrate-induced Changes in Protein Abundance Measured by iTRAQ Quantification—Treatment of rodents with bezafibrate causes a general augmentation of the peroxisomal compartment as well as a remodeling of the enzymatic pattern of the organelles, leading to an enhanced capacity to sequester long and very long chain fatty acids in the liver. This process is reflected by the differential expression of peroxisomal proteins in our study.

The iTRAQ values imply that a number of peroxins were induced in the liver of bezafibrate-treated rats compared with control animals. Highest induction rates were observed for Pex11α, a peroxin implicated in the process of membrane fission (Table 4).

As expected, we also observed a significant increase in putative enzymes of β-oxidation of straight long chain fatty acids (C16–C18), *e.g.* the L-bifunctional enzyme (L-PBE) or the 3-ketoacyl-CoA thiolase after bezafibrate treatment. In contrast, the corresponding enzymes of the β-oxidation of very long straight chain fatty acids, the D-bifunctional enzyme (D-PBE), ALDP, the very long chain acyl-CoA synthetase, and the thiolase harboring SCPX were only induced to a lower extent or even down-regulated. This is in line with the low β-oxidation rates found for lignoceroyl-CoA compared with palmitoyl-CoA in both the induced and un-induced state (Table 3). Apparently, MS allows for the detection of changes in the regulation of entire metabolic pathways. With respect to the total mass of peroxisomal proteins, ACOX1 was not or only slightly induced but remained stable after fibrate treatment. Similar results were shown for ACOX2 and ACOX3 (Table 4). Furthermore, the enzyme activities of ACOX1 for the oxidation of palmitoyl-CoA were also comparable in bezafibrate-treated and control animals (24.83 *versus* 24.13 units/mg protein). The remaining peroxisomal enzymes involved in lipid metabolism increased upon fibrate treatment further substantiating that liver peroxisomes remodel their enzymatic composition predominantly, to effectively sequester unbranched long chain fatty acids. Enzymes for the entire pathway, including potential transporters such as PMP70, proteins for storage of fatty acids like fatty acid-binding protein p14, the peroxisomal acyl-CoA thioesterase 4 (ACOT4), or different carnitine acyltransferases involved in transfer of shortened fatty acyl-CoAs to mitochondria, also were all increased by bezafibrate treatment (Table 4).

Localization of Newly Identified Peroxisomal Matrix Proteins—To substantiate the identification of newly identified peroxisomal proteins, we focused on the analysis of proteins fused with the Myc or FLAG epitope. Epitope-tagged proteins were expressed in CHO cells (BGL69) with constitutive expression of a GFP-PTS1 fusion protein for visualization in peroxisomes. For proteins with a predicted PTS1 sequence (Table 5), we investigated only protein variants with an N-terminal tag. For all other proteins, N- as well as C-terminal fusions with epitope tags were constructed to preserve possible targeting information located at the termini of the proteins. We found that EBP50 (Q9JJ19), a presumed cytosolic protein with a PTS1 signal in its peptide sequence, was localized almost exclusively to peroxisomes when expressed in BGL69 cells in moderate amounts (see Fig. 2, *A–C*) sug-

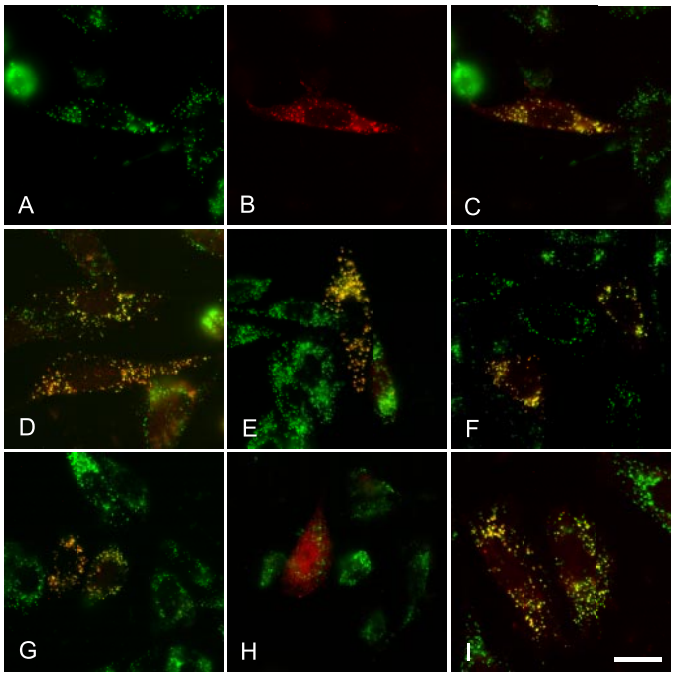

FIGURE 2. **Newly identified proteins are localized to peroxisomes.** Plasmids for expression of Myc-tagged proteins were transiently transfected into BGL69 cells that already express a GFP-PTS1 fusion protein for visualization of peroxisomes (*green* signal in *A*). The Myc epitope was visualized immunocytochemically (*red signal* in *B*). Colocalization of the Myc epitope with GFP-PTS1 in overlays of images *A* and *B* is indicated by *yellow signals* (*C*). Cells in *A–C* were transfected with a plasmid for expression of a N-myc-EBP50 fusion protein. *D–I*, only the overlays of images for GFP (*green*) and the localization of the following proteins (*red*) are shown. *D*, N-myc-Tysnd1; *E*, N-myc-Zn ADH; *F*, N-myc-acyl-CoA dehydrogenase family member 11, *G*, N-myc-δ3,δ2-enoyl CoA isomerase; *H*, N-myc-lactamase β2; and *I*, C-myc-ACBD5.1. Note the almost complete colocalization of proteins with the peroxisomal marker GFP-PTS1 except for image *H*. As shown for the gene product of lactamase β2 (*H*), a PTS1 signal sequence does not guarantee a peroxisomal localization; however, the existence of splice variants, which are targeted to peroxisomes via this PTS1, cannot be excluded. All images show the same magnification; the *bar* in *I* represents 20 μm.

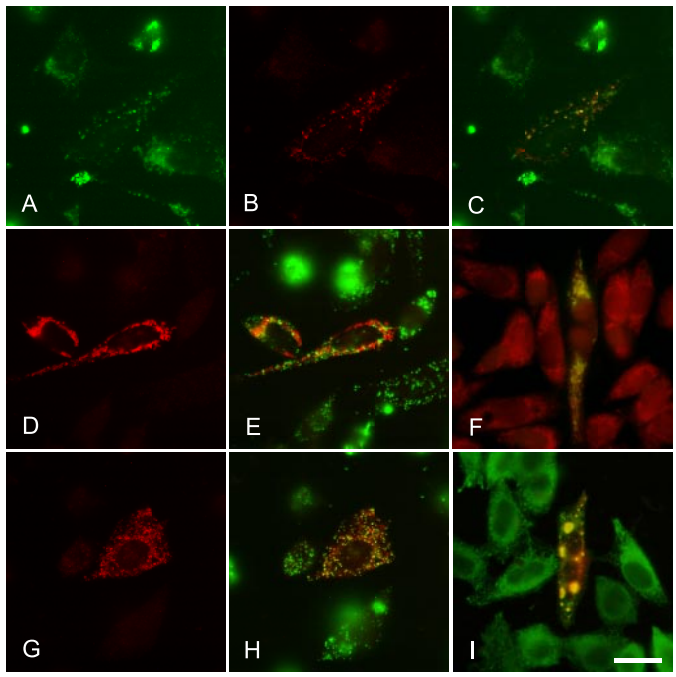

FIGURE 3. **Localization of proteins can vary with the position of the epitope tag and the level of expression.** Plasmids for expression of Myc-tagged proteins were transiently transfected into CHO cells (*F*) or into BGL69 cells (all except *F*) with GFP-labeled peroxisomes (*green signal* in *A*). The Myc epitope was visualized immunocytochemically (*red signal* in *B–E* and *G–I* or *green signal* in *F*). A colocalization of the green and red signals in overlays (*C, E, F, H,* and *I*) of corresponding images is indicated by *yellow signals*. Cells in *A–C* were transfected with a plasmid for expression of a C-myc-Mosc domain containing protein 2 fusion. *D–F*, localization of a N-myc Mosc domain containing protein 2 fusion is shown. *F*, mitochondria of CHO cells were labeled in *red*, and the Myc epitope was labeled in *green*. Note the complete overlap of the signals. *G–I*, cells were transfected with plasmids for expression of an N-myc-Dhrs7b fusion proteins. *G* and *H* show the initially published version Dhrs7b.1 fused to an N-terminal Myc tag; *I* represents the splice variant N-myc-Dhrs7b.2, which colocalizes with a concanavalin A staining (*red*) used to mark the endoplasmic reticulum. All images show the same magnification; the *bar* in *I* represents 20 μm.

gesting that this protein possesses a functional PTS1. However, when expressed at higher levels, it was also found in the cytosol (not shown), where it has been described originally as a scaffolding protein attached to proteins of the ezrin-radixin-moesin family (30). Similarly, trypsin domain containing 1 (XP_345107.1, Tysnd1), the acyl-CoA dehydrogenase family member 11 (Q80XL6), the δ3,δ2-enoyl-CoA isomerase (NP_001009275), and the zinc-binding alcohol dehydrogenase domain containing 2 (XP_214526, Zn-ADH) were all targeted to peroxisomes, when fused with a Myc epitope at their N terminus (see Fig. 2, *D–G*). However, not all identified proteins with a PTS1 in their predicted peptide sequence were localized to peroxisomes. The potential lactamase β2 (NP_663356) ending with the amino acids AVL at its C terminus was not localized to a specific subcellular structure upon expression in BGL69 cells, demonstrating that a PTS1 analog-targeting sequence is not always a guarantee for peroxisomal import (Fig. 2*H*).

Localization of Newly Identified Peroxisomal Membrane Proteins—For newly identified proteins without an obvious peroxisomal targeting sequence, *e.g.* the Mosc domain containing protein 2, the subcellular localization was dependent on the position of the epitope tag. The Mosc domain containing protein 2 (O88994) was mostly localized to peroxisomes when fused with a C-terminal Myc tag (Fig. 3, *A–C*). However, when the Myc epitope was fused to the N terminus of the protein, most of the Myc immunoreactivity did not colocalize with peroxisomes (Fig. 3, *D* and *E*). Instead, the fusion protein was localized to mitochondria, demonstrated by overlap of the immunolabeling with a mitochondrial marker shown in Fig. 3*F*. This is in line with a predicted mitochondrial targeting sequence from amino acids 1–35 as described in SwissProt. Because peroxisomal membrane protein targeting sequences are highly variable, it can only be speculated that the N-terminal tag disturbs the targeting signal; however, a couple of membrane protein targeting sequences localize at least in part to the N terminus (31).

The subcellular localization of the short chain dehydrogenase 7b (Q8VID1, Dhrs7b.1) was altered by its level of expression. When expressed at low levels, judged from the fluorescence intensity of the immunostaining, an N-myc-Dhrs7b.1 fusion was localized mostly to peroxisomes (Fig. 3, *G* and *H*). Upon higher expression, however, most of the Myc immunostaining did not colocalize with GFP-PTS1 as the marker of peroxisomes (not shown). A Dhrs7b fusion with the Myc epitope at its C terminus did not localize to peroxisomes when expressed in CHO cells (not shown). We also identified a splice

variant of the short chain dehydrogenase 7b (Dhrs7b.2, accession number EF445633). An N-myc-Dhrs7b.2 fusion was localized to the endoplasmic reticulum shown by colocalization with concanavalin A (Fig. 3*I*) as predicted by the software PSORTII. Expression of the N-myc-Dhrs7b.2-fusion induced a reorganization of the endoplasmic reticulum demonstrated by the aberrant concanavalin A staining pattern with a focal concentration of the staining in several areas of N-myc-Dhrs7b.2-expressing cells (Fig. 3*I*).

Among the new peroxisomal membrane proteins, we have also identified proteins that caused alterations of the peroxisomal morphology when expressed in BGL69 cells. A C-terminally Myc-tagged version of the PMP52 (NP_001013918) was colocalized with GFP-PTS1, indicating its association with peroxisomes (Fig. 4, *A–C*). However, as a result of the PMP52 expression, the number of peroxisomes was dramatically reduced, and a significant portion of the GFP-PTS1 was localized in the cytoplasm, indicating that its import was impaired. The same result was obtained upon expression of PMP52 bearing a N-terminal Myc tag (not shown). To exclude that the alterations of peroxisomal import and morphology were attributed to expression of artificial fusion proteins, we have also analyzed BGL69 cells overexpressing the wild-type PMP52. An expression vector for PMP52 was cotransfected with pGHL252, a vector for a RFP-PTS1 fusion protein, to visualize transfected cells (Fig. 4, *D–F*). Indeed, the latter showed the same alterations with a reduced number of peroxisomes and an impaired import of GFP-PTS1 suggesting that low expression rates are crucial for its physiological function. To quantify the frequency of the PMP52-induced phenotype, we compared peroxisome morphology and the localization of the GFP-PTS1 in BGL69 cells after cotransfection with the RFP-PTS1 and the PMP52 expression vector with that of BGL69 cells transfected with the RFP-PTS1 vector alone. Analysis of 100 RFP-PTS1 transgenic cells showed alterations of peroxisome morphology and cytoplasmic GFP localization in 89% of transgenic cells after cotransfection, and only in 3% of transgenic cells of the controls after transfection of the RFP-PTS1 alone. This observation indicates that the alteration of the peroxisomal compartment was indeed because of expression of wild-type PMP52.

By 5′ rapid amplification of cDNA ends-PCR, we cloned two splice variants of the acyl-CoA-binding protein ACBD5, named ACBD5.1 (EF026991), lacking exon 1, and ACBD5.2 (EF026992). A slightly different effect on peroxisome morphology was observed upon expression of both variants of ACBD5. ACBD5.2 tagged with an N-terminal Myc epitope caused a tubular elongation of peroxisomes in BGL69 cells. The GFP-PTS1 colocalized with the tubular Myc immunolabeling but was mostly concentrated in dot-like beads on a string (Fig. 4, *G–I*). Again, the same result was obtained by expression of ACBD5.2 tagged with a C-terminal Myc epitope (not shown). Furthermore, the transient expression of the wild-type ACBD5.2 cotransfected with a DsRed expression vector for visualization of transfected cells also caused the same phenotype (Fig. 4, *J–L*), suggesting an interference with the physiological fission process. The ACBD5.1 was also localized to peroxisomes (Fig. 2*I*). We observed an induction of rod-like peroxisomes in a fraction of ACBD5.1-expressing cells (not shown), but the phenotype was much less pronounced compared with that caused by ACBD5.2 overexpression.

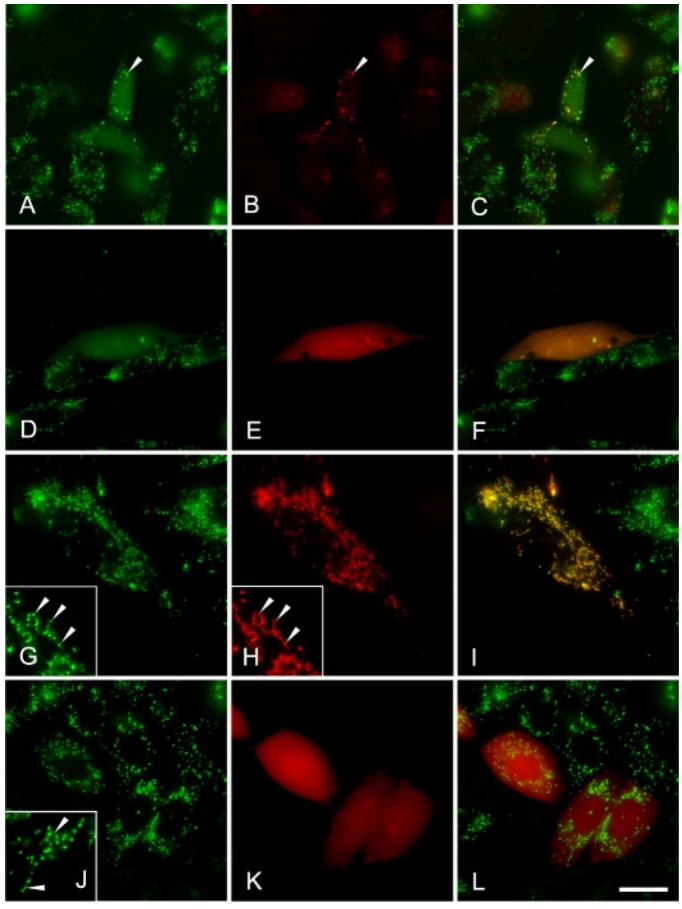

FIGURE 4. **Overexpression of newly identified peroxisomal membrane proteins affects peroxisome morphology and import of peroxisomal proteins.** BGL69 cells with GFP-labeled peroxisomes (*green* in *A, D, G,* and *J*) were transfected with plasmid for expression of the following proteins. *A–C,* C-myc-PMP52; *D–F,* PMP52 and DsRed; *G–I,* N-myc ACBD5.2; or *J–L,* ACBD5.2 and DsRed. The Myc epitopes (*B* and *H*) and the DsRed (*E* and *K*) are shown in *red.* Overlays of corresponding images are shown in *C, F, I,* and *L*. Note the reduced number of PMP52-positive peroxisomes (*arrowhead* in *A–C*) and the cytoplasmic localization of GFP-PTS1 in transfected cells (*C* and *D*). Note also the appearance of elongated N-myc-ACBD5.2-positive peroxisomes (*arrowheads* in *insets* of *G* and *H*) as well as of similar structures in cells transfected with a plasmid for expression of ACBD5.2 (*inset* in *J*). All images show the same magnification; the *bar* in *L* represents 20 μm.

DISCUSSION

The objective of this study was to characterize the proteome of rat liver peroxisomes and to register regulative changes in the peroxisomal protein pattern after treatment of rats with the hypolipidemic drug bezafibrate. We chose this system to identify previously undescribed proteins, to link selected data from the literature to an experiment at the organellar proteome level to validate this quantitative approach, and to obtain a more complex view of the alterations induced by hypolipidemic drugs. Although proteomic profiling cannot replace metabolic studies and detailed functional analyses, it can be a hypotheses-generating instrument, giving rise to new cell biological ideas by carefully interpreting the large amounts of data.

Quantitative Mass Spectrometry—For most peroxisomal proteins, the iTRAQ analysis revealed that their abundance

remained more or less constant in both control and fibrate-treated animals if referred to the total amount of peroxisomal protein. In relation to the total mass of liver protein, however, peroxisome proliferation leads to an increased expression of most peroxisomal proteins concomitant with corresponding changes at the transcriptional level (32–35). However, the iTRAQ quantification values also indicated specific alterations of protein induction, when calculated per peroxisomal protein. Although peroxins responsible for the import of matrix and membrane proteins (Pex3, see Ref. 36) were both moderately elevated (1.3–1.4 times), higher rates were found for Pex16 (1.75 times) and Pex11α (~2.6 times), involved in early peroxisome membrane assembly (37, 38) and peroxisome proliferation, respectively (39).

Modulations in the content of peroxisomal enzymes commonly imply a shift in their ability to sequester specific fatty acid substrates (40). This notion is substantiated by the high induction rates of the high abundant proteins L-PBE, the 3-ketoacyl-CoA thiolase, and the potential fatty acid transporter PMP70 and the low to moderate ones of D-PBE, ALDP, and the very long chain acyl-CoA synthetase (Table 4). As the D-PBE promoter bears a clear PPARα-response element, these finding may appear contradictory. Yet as is repeatedly reported, the D-PBE is only less induced compared with L-PBE (see Ref. 41 for review), which may reflect a more modular response of the D-PBE to different PPARα ligands. Using a knock-out mouse model, Baes *et al.* (42) elegantly showed that only the D-PBE takes part in the oxidation of very long chain fatty acids (C22–C26), whereas the L-PBE would sequester preferentially long chain fatty acid substrates (C16–C18). Thus, our data verify the hypothesis of Kikuchi and co-workers (43) that long chain fatty acids are the major substrates of rat liver peroxisomes with the corresponding enzymes induced by the fibrate treatment. In contrast, the abundance of enzymes for β-oxidation of very long chain fatty acids is comparatively low in both the induced and un-induced state. In this context, it is interesting that PMP70 is the only ABC half-transporter with a high concentration in rat liver and a quite high induction rate, arguing for its involvement in transport of long chain fatty acids (C16–C18) across the peroxisomal membrane (see Ref. 44 for review). Until now, however, only its role in the transport of bile acid metabolites and branched chain fatty acids has been indicated (45), the pathways found to be down-regulated or unresponsive to bezafibrate in this study. Thus, in summary, fibrate treatment in rodents induced highly specific changes in peroxisomal enzyme content and metabolism (Tables 3 and 4), supporting the view of a modifiable signal transduction of the PPARα receptor in response to different ligands, potentially by ligand-dependent interaction with variable cofactors.

The ACOX1 has been described as the rate-limiting enzyme of β-oxidation (46, 47). We found that its abundance remained more or less stable upon bezafibrate treatment in both immunoblot and iTRAQ data when calculated per peroxisomal protein amount. At a first glance, this observation seems to contradict previous investigations, where ACOX1 was also augmented (48). However, in comparison to L-PBE and 3-ketoacyl-CoA thiolase, ACOX1 induction rates were generally found to be low when measured in isolated peroxisomes (9). Because bezafibrate-induced protein changes are dose- as well as time-dependent (49), the moderate enzyme induction observed in our study might be related to the distinct routes of bezafibrate application, normal food intake here *versus* gastric intubation in other studies. Nevertheless, the distinct induction pattern of ACOX1 compared with other enzymes of the β-oxidation pathway raises the question of how the metabolic flux of fatty acid breakdown is regulated. Primarily, the pronounced induction of the consecutive enzymes points toward a rapid conversion of the downstream metabolites, preventing the organelle from accumulation of 3-hydroxyacyl- or ketoacyl-CoA esters. Indeed, Osumi *et al.* (50) reported an inhibition of rat ACOX1 by 3-ketohexadecanoyl-CoA at a K_i of 0.47 μM. Because the K_m value of the 3-ketoacyl-CoA thiolase is 1.9 μM (51), high induction rates of the enzymes of the 2nd and 3rd step of peroxisomal β-oxidation may prevent ACOX1 from product inhibition during phases of increased fatty acid breakdown. These findings are in line with the observations of Aoyama *et al.* (52) indicating that enhanced β-oxidation rates because of ACOX1 overexpression are confined to cell lines with low ACOX1 content. Because rat liver peroxisomes contain relatively high concentrations of ACOX1 (53), a strong induction could lead to inhibitory concentrations of β-oxidation products reducing its enzymatic activity. Moreover, ACOX1 is also inhibited by acetyl-CoA (54). One of the mechanisms competing with this inhibition could be the induction of peroxisomal carnitine acetyl- as well as acyltransferases supporting a rapid export of chain-shortened fatty acids to the mitochondria for their final metabolization. In addition, the up-regulated fatty acid-binding protein p14, which was localized to peroxisomes recently (55), could bind, solubilize, and deliver these mobilized non-esterified fatty acids to the peroxisomal membrane, where they can be converted to their carnitine derivatives by carnitine octanoyltransferase. Extending this view, the supply and availability of CoASH as another regulating factor should be mentioned, because for every chain-shortening event another coenzyme A is consumed. Peroxisomes house an internal pool of CoASH, which cannot diffuse across the organellar membrane (56, 57). Horie *et al.* (58) have found an increase in free CoASH upon fibrate stimulation, whereas acyl-bound CoA remained stable, concluding that the free CoASH concentration is a positive regulating factor in the enhancement of the peroxisomal fatty acid oxidation system. As described by Hunt *et al.* (59), the peroxisomal acyl-CoA thioester hydrolase Ib, up-regulated in our study, shows high affinities to acetyl-CoA. The induction of this enzyme could force the recruitment of free CoASH through the hydrolysis of acetyl-CoA otherwise accumulating in the peroxisomal matrix. In parallel to an internal mobilization of CoASH, the up-regulated cytosolic thioesterases could provide additional coenzyme A to be imported into the organelle by a yet uncharacterized transport system. Hence, our data support the view that free CoASH could be a rate-limiting factor during bezafibrate-induced β-oxidation. In summary, the

enhanced rates of β-oxidation of palmitoyl-CoA upon bezafibrate treatment, from 16.98 to 45.45 milliunits/mg (Table 3), might not only be accounted for by a mere numerical increase of peroxisomal enzymes but supposedly also by a streamlined close control of the intraorganellar flux.

Potential Functions of Newly Identified Peroxisomal Proteins—Among the newly identified peroxisomal proteins, a number of dehydrogenases/reductases were found. Judged from the number of peptide identifications one of the most prominent is the acyl-CoA dehydrogenase family member 11. Similar peptide counts were only obtained for enzymes of major peroxisomal pathways like the ACOX1 or the ketoacyl-CoA thiolase. This potential acyl-CoA dehydrogenase was also found by Kikuchi *et al.* (43) but has not yet been verified by cloning and colocalization experiments. This enzyme bears two functional domains, a phosphotransferase as well as an acyl-CoA dehydrogenase domain that is distantly related to the mitochondrial medium chain acyl-CoA dehydrogenases (27% identities in the acyl-CoA dehydrogenase domain). Because peroxisomal acyl-CoA oxidases are related to this protein family (60), it remains to be clarified whether this enzyme acts as a dehydrogenase or whether it is a fourth acyl-CoA oxidase, potentially broadening the substrate spectrum of peroxisomal β-oxidation.

In addition to metabolic enzymes we detected proteins with more basic potential functions in peroxisome maintenance. Molybdopterin cofactor sulfurases usually provide a sulfur atom for the molybdopterin cofactor or other metallo-sulfur clusters (61). Because xanthine oxidase, which is located to peroxisomes in rodents (62), is a molybdopterin cofactor-using protein, the newly identified Mosc domain containing protein 2 could be an essential enzyme for the transfer of a sulfur group to this protein. Indeed, the disruption of a human sulfur transferase was reported to lead to xanthinuria (63). Interestingly, this protein was recently annotated in SwissProt as a complex with cytochrome b_5 and cytochrome b_5 reductase (O88994). Because both proteins are consistently identified in peroxisomal liver samples (19, 23, 43), it has to be speculated if this complex is also formed in peroxisomes.

The existence of a peroxisomal protease has been proposed for decades. We detected a trypsin-like serine protease (MGC34695, Tysnd1) in addition to the peroxisomal Lon protease (43), which extends the potential of the organelles to degrade endogenous proteins. During submission of this manuscript, Kurochkin and co-workers (64) identified and characterized the mouse variant of this protein. By using overexpression experiments, the authors could show that Tysnd1 is involved in the controlled cleavage of peroxisomal matrix proteins such as ACOX1, D-PBE, SCPX, and the 3-ketoacyl-CoA thiolase. The authors speculate that Tysnd1 could take part in enhancing β-oxidation by facilitating the formation of multiprotein complexes modulating the secondary structure of individual constituents through enzymatic cleavage of otherwise inhibiting subgroups. Supporting these findings Tysnd1 was up-regulated by a factor of 2 after a 3-week treatment with high doses of bezafibrate. In our experiments, however, Tysnd1 proved not to be up-regulated using lower doses and a shorter time period. In addition, a characterization of the ACOX1 tertiary structure using two-dimensional blue native-PAGE (65) revealed that this key component of the β-oxidation chain can only be found as a complex consisting of both precursor and cleaved subunits A–C. In contrast, complexes consisting only of completely processed polypeptides seem not to be present in peroxisomes (supplemental Fig. S2), which suggests a more complex regulating mechanism. Interestingly, in humans two isoforms of Tysnd1 can be found as GenBank™ splice variants, one lacking the C-terminal SKL sequence. Because we detected another trypsin-like protein sequence, which lacks any peroxisomal targeting sequence (Table 4), the existence of further proteases, existing as previously undiscovered splice variants, cannot be excluded.

We have also identified a new peroxisomal membrane protein PMP52 with five predicted transmembrane domains in TMHMM (NP_001013318) that may fulfill a task in the process of peroxisome maintenance. So far, PMP52 has no apparent functional domains, which would specify a relation to a known protein family. However, overexpression of PMP52 in CHO cells caused alterations in peroxisome number and morphology affecting the import competence of the whole peroxisomal compartment. The PMP52-induced changes were similar to characteristic morphological changes observed upon induced degradation of the peroxisomal compartment in CHO cells.[4] Thus, PMP52 could be involved in the control of the turnover of peroxisomes. A PSI-Blast search disclosed a weak but significant relationship to the mammalian PMP24 (30% identity in the aligned sequence), another peroxisomal membrane protein with no assigned function (66). Concerning evolutionary conservation, both proteins exist in deuterostomia as well as fungi. In contrast, in protostomia (arthropods) as well as plants only PMP52-like sequences exist, whereas PMP24 seems to be abandoned, suggesting a functional overlap of both proteins.

Kikuchi and co-workers (43) first mentioned the acyl-CoA-binding protein RiK1300014E15, now classified as ACBD5, as a peroxisomal constituent. However, the authors concluded that this peptide sequence is the precursor protein of the 10-kDa acyl-CoA-binding protein, which is activated by PPARs (67). In the meantime, a whole gene family of proteins bearing an acyl-CoA binding domain (ACBD1–5) has been sequenced. According to the Pfam-data base ACB domains bind medium and long chain fatty acids with very high affinities and thus may fulfill important functions in peroxisomes to be investigated. We cloned two forms of ACBD5 and confirmed peroxisomal localization for both by coexpression experiments. Because we identified the protein only in the integral membrane fraction, we searched for potential membrane domains using the TMHMM software. The prediction of a single transmembrane domain is in line with studies of *Arabidopsis thaliana* acyl-CoA-binding proteins, which are also membrane-associated proteins (68). However, because only the acyl-CoA binding domain is evolutionarily conserved between both phyla, these membrane domains must have developed independently as functional

[4] G. H. Lüers, unpublished observations.

analogues. Besides the acyl-CoA binding domain ranging from amino acids 44–132 (PF00887), ACBD5 shows only regions of low complexity impeding further functional speculations. Interestingly, overexpression of ACBD5.2 and ACBD5.1 in CHO cells leads to an elongation of peroxisomes, which is similar to the appearance of peroxisomes after arachidonic acid treatment in HepG2 cells (69). The commonly accepted concept of nuclear control of peroxisome proliferation via PPARα was recently questioned by Zhang and co-workers (70), who demonstrated peroxisome proliferation in PPARα-null mice. Thus, ACBD5 may influence peroxisomal proliferation directly, potentially linking the abundance of cellular acyl-CoA to the peroxisomal fission events.

In summary, the combination of diverse techniques ranging from quantitative MS to cloning and the expression of epitope-tagged fusion proteins and to immunocytochemical analysis of their localization lead to the identification of several new peroxisomal proteins besides the already known ones, thus adding new pieces to the mosaic of the of rat liver peroxisomal proteome. The potential integration of new proteins such as PMP52 or ACBD5 into aspects of biogenesis and turnover of the organelle could pave the way for further functional studies. With the modulation of the β-oxidation enzymes and related proteins (acyl-CoA thioesterases) upon the treatment with bezafibrate, new light was shed on the differential regulation of peroxisomal β-oxidation pathways. Thus, quantitative mass spectrometry promises to be a valuable extension to established biochemical and molecular techniques, able to add new functional aspects to long investigated areas of research.

Acknowledgments—We thank Prof. Dr. H. D. Fahimi for carefully proofreading this manuscript. The excellent technical assistance of H. Mohr, K. Rummer, A. Cordes, and C. Fieger is greatly acknowledged. We thank Prof. R. A. Wanders for the kind donation of lignoceroyl-CoA.

REFERENCES

1. Raymond, G. V. (1999) *Curr. Opin. Pediatr.* **11,** 572–576
2. Moser, H. W. (2000) *Front. Biosci.* **5,** D298–D306
3. Schluter, A., Fourcade, S., Domenech-Estevez, E., Gabaldon, T., Huerta-Cepas, J., Bertthommler, G., Ripp, R., Wanders, R. J., Poch, O., and Pujol, A. (2007) *Nucleic Acids Res.* **35,** D815–D822
4. Lazarow, P. B., and De Duve, C. (1976) *Proc. Natl. Acad. Sci. U. S. A.* **73,** 2043–2046
5. Lazarow, P. B., Fujiki, Y., Mortensen, R., and Hashimoto, T. (1982) *FEBS Lett.* **150,** 307–310
6. Fahimi, H. D., Reinicke, A., Sujatta, M., Yokota, S., Ozel, M., Hartig, F., and Stegmeier, K. (1982) *Ann. N. Y. Acad. Sci.* **386,** 111–135
7. Leighton, F., Coloma, L., and Koenig, C. (1975) *J. Cell Biol.* **67,** 281–309
8. Moody, D. E., and Reddy, J. K. (1976) *J. Cell Biol.* **71,** 768–780
9. Beier, K., Völkl, A., Hashimoto, T., and Fahimi, H. D. (1988) *Eur. J. Cell Biol.* **46,** 383–393
10. Chen, N., and Crane, D. I. (1992) *Biochem. J.* **283,** 605–610
11. Kovacs, W., Stangl, H., Völkl, A., Schad, A., Fahimi, H. D., and Baumgart, E. (2001) *Eur. J. Biochem.* **268,** 4850–4859
12. Ong, S. E., and Mann, M. (2005) *Nat. Chem. Biol.* **1,** 252–262
13. Wu, C. C., MacCoss, M. J., Howell, K. E., and Yates, J. R., III (2003) *Nat. Biotechnol.* **21,** 508–510
14. Goshe, M. B., Blonder, J., and Smith, R. D. (2003) *J. Proteome Res.* **2,** 153–161
15. Bagshaw, R. D., Mahuran, D. J., and Callahan, J. W. (2005) *Mol. Cell. Proteomics* **4,** 133–143
16. Schirmer, E. C., and Gerace, L. (2005) *Trends Biochem. Sci.* **30,** 551–558
17. Andersen, J. S., and Mann, M. (2006) *EMBO Rep.* **7,** 874–879
18. Völkl, A., and Fahimi, H. D. (1985) *Eur. J. Biochem.* **149,** 257–265
19. Weber, G., Islinger, M., Weber, P., Eckerskorn, C., and Voelkl, A. (2004) *Electrophoresis* **25,** 1735–1747
20. Li, W., and Godzik, A. (2006) *Bioinformatics* (*Oxf.*) **22,** 1658–1659
21. Kyhse-Andersen, J. (1984) *J. Biochem. Biophys. Methods* **10,** 203–209
22. Small, G. M., Burdett, K., and Connock, M. J. (1985) *Biochem. J.* **227,** 205–210
23. Islinger, M., Lüers, G. H., Zischka, H., Ueffing, M., and Völkl, A. (2006) *Proteomics* **6,** 804–816
24. Alexson, S. E., Fujiki, Y., Shio, H., and Lazarow, P. B. (1985) *J. Cell Biol.* **101,** 294–304
25. Hogenboom, S., Wanders, R. J., and Waterham, H. R. (2003) *Mol. Genet. Metab.* **80,** 290–295
26. Morel, F., Rauch, C., Petit, E., Piton, A., Theret, N., Coles, B., and Guillouzo, A. (2004) *J. Biol. Chem.* **279,** 16246–16253
27. Remacle, J., Fowler, S., Beaufay, H., Amarcostesec, A., and Berthet, J. (1976) *J. Cell Biol.* **71,** 551–564
28. Fowler, S., Remacle, J., Trouet, A., Beaufay, H., Berthet, J., Wibo, M., and Hauser, P. (1976) *J. Cell Biol.* **71,** 535–550
29. Miyauchi, K., Yamamoto, A., Masaki, R., Fujiki, Y., and Tashiro, Y. (1993) *Cell Struct. Funct.* **18,** 427–436
30. Reczek, D., Berryman, M., and Bretscher, A. (1997) *J. Cell Biol.* **139,** 169–17930
31. van Ael, E., and Fransen, M. (2006) *Biochim. Biophys. Acta* **1763,** 1629–1638
32. Cornwell, P. D., De Souza, A. T., and Ulrich, R. G. (2004) *Mutat. Res.* **549,** 131–145
33. Baker, V. A., Harries, H. M., Waring, J. F., Duggan, C. M., Ni, H. A., Jolly, R. A., Yoon, L. W., De Souza, A. T., Schmid, J. E., Brown, R. H., Ulrich, R. G., and Rockett, J. C. (2004) *Environ. Health Perspect.* **112,** 428–438
34. Yadetie, F., Laegreid, A., Bakke, I., Kusnierczyk, W., Komorowski, J., Waldum, H. L., and Sandvik, A. K. (2003) *Physiol. Genomics* **15,** 9–19
35. Richert, L., Lamboley, C., Viollon-Abadie, C., Grass, P., Hartmann, N., Laurent, S., Heyd, B., Mantion, G., Chibout, S. D., and Staedler, F. (2003) *Toxicol. Appl. Pharmacol.* **191,** 130–146
36. Ghaedi, K., Tamura, S., Okumoto, K., Matsusono, Y., and Fujiki, Y. (2000) *Mol. Biol. Cell.* **11,** 2085–2102
37. Honsho, M., Hiroshige, T., and Fujiki, Y. (2002) *J. Biol. Chem.* **277,** 44513–44524
38. Fang, Y., Morell, J. C., Jones, J. M., and Gould, S. J. (2004) *J. Cell Biol.* **164,** 863–875
39. Thoms, S., and Erdmann, R. (2005) *FEBS J.* **272,** 5169–5181
40. Lazarow, P. B. (1977) *Science* **197,** 580–581
41. Huyghe, S., Mannaerts, G. P., Baes, M., and Van Veldhoven, P. P. (2006) *Biochim. Byophys. Acta* **1761,** 973–994
42. Baes, M., Huyghe, S., Carmeliet, P., Declercq, P. E., Collent, D., Mannaerts, G. P., and van Veldhoven, P. P. (2000) *J. Biol. Chem.* **275,** 16329–16336
43. Kikuchi, M., Hatano, N., Yokota, S., Shimozawa, N., Imanaka, T., and Taniguchi, H. (2004) *J. Biol. Chem.* **279,** 421–428
44. Wanders, R. J. A., and Waterham, H. R. (2006) *Annu. Rev. Biochem.* **75,** 295–332
45. Visser, W. F., van Roermund, C. W. T., Ijlst, L., Waterham, H. R., and Wanders, R. J. A. (2007) *Biochem. J.* **401,** 365–375
46. Inestrosa, N. C., Bronfman, M., and Leighton, F. (1979) *Life Sci.* **25,** 1127–1135
47. Hryb, D. J., and Hogg, J. F. (1979) *Biochem. Biophys. Res. Commun.* **87,** 1200–1206
48. Nemali, M. R., Usuda, N., Reddy, M. K., Oyasu, K., Hashimoto, T., Osumi, T., Rao, M. S., and Reddy, J. K. (1988) *Cancer Res.* **48,** 5316–5324
49. Pill, J., Völkl, A., Hartig, F., and Fahimi, H. D. (1992) *Arch. Toxicol.* **66,** 327–333
50. Osumi, T., Hashimoto, T., and Ui, N. (1980) *J. Biochem.* (*Tokyo*) **87,** 1735–1746
51. Miyazawa, S., Furuta, S., Osumi, T., Hashimoto, T., and Ui, N. (1981)

J. Biochem. (*Tokyo*) **90,** 511–519
52. Aoyama, T., Souri, M., Kamijo, T., Ushikubo, S., and Hashimoto, T. (1994) *Biochem. Biophys. Res. Commun.* **201,** 1541–1547
53. Bell, D. R., Bars, R. G., and Elcombe, C. R. (1992) *Eur. J. Biochem.* **206,** 979–986
54. Hovik, R., and Osmundsen, H. (1989) *Biochem. J.* **263,** 297–299
55. Antonenkov, V. D., Sormunen, R. T., Ohlmeier, S., Amery, L., Fransen, M., Mannaerts, G. P., and Hiltunen, J. K. (2006) *Biochem. J.* **394,** 475–484
56. Van Broekhoven, A., Peeters, M. C., Debeer, L. J., and Mannaerts, G. P. (1981) *Biochem. Biophys. Res. Commun.* **100,** 305–312
57. Antonenkov, V. D., Sormunen, R. T., and Hiltunen, J. K. (2004) *J. Cell Sci.* **117,** 5633–5642
58. Horie, S., Isobe, M., and Suga, T. (1986) *J. Biochem.* (*Tokyo*) **99,** 1345–1352
59. Hunt, M. C., Solaas, K., Kase, B. F., and Alexson, S. E. (2002) *J. Biol. Chem.* **277,** 1128–1138
60. Latruffe, N., and Vamecq, J. (2000) *Biol. Cell* **92,** 389–395
61. Anantharaman, V., and Aravind, L. (2002) *FEMS Microbiol. Lett.* **207,** 55–61
62. Angermüller, S., Bruder, G., Völkl, A., Wesch, H., and Fahimi, H. D. (1987) *Eur. J. Cell Biol.* **45,** 137–144
63. Ichida, K., Matsumura, T., Sakuma, R., Hosoya, T., and Nishino, T. (2001) *Biochem. Biophys. Res. Commun.* **282,** 1194–1200
64. Kurochkin, I. V., Mizuno, Y., Konagaya, A., Sakaki, Y., Schönbach, C., and Okazaki, Y. (2007) *EMBO J.* **26,** 835–845
65. Schägger, H., Cramer, W. A., and von Jagow, G. (1994) *Anal. Biochem.* **217,** 220–230
66. Reguenga, C., Oliveira, M. E., Gouveia, A. M., Eckerskorn, C., Sa-Miranda, C., and Azevedo, J. E. (1999) *Biochim. Biophys. Acta* **1445,** 337–341
67. Helledie, T., Grontved, L., Jensen, S. S., Kiilerich, P., Rietveld, L., Albrektsen, T., Boysen, M. S., Nohr, J., Larsen, L. K., Fleckner, J., Stunnenberg, H. G., Kristiansen, K., and Mandrup, S. (2002) *J. Biol. Chem.* **277,** 26821–26830
68. Li, H. Y., and Chye, M. L. (2003) *Plant Mol. Biol.* **51,** 483–492
69. Schrader, M., Krieglstein, K., and Fahimi, H. D. (1998) *Eur. J. Cell Biol.* **75,** 87–96
70. Zhang, X., Tanaka, N., Nakajima, T., Kamijo, Y., Gonzalez, F. J., and Aoyama, T. (2006) *Biochem. Biophys. Res. Commun.* **346,** 1307–1311